CONEM 2022
CONGRESSO NACIONAL DE ENGENHARIA MECÂNICA
TERESINA - PI

ABCM
XI CONGRESSO NACIONAL DE ENGENHARIA MECÂNICA
DE 07 A 11 DE AGOSTO DE 2022, TERESINA-PI, BRASIL

# EXPERIMENTAL AND NUMERICAL STUDY OF TWO-PHASE SLUG FLOW IN A LONG VERTICAL PIPE

**Gabriela Pereira Toledo, toledop.gabriela@gmail.com**
**Ricardo Augusto Mazza, mazza@fem.unicamp.br**

Faculty of Mechanical Engineering – University of Campinas, Rua Mendeleyev 200, 13083-860, Campinas, SP, Brazil

***Abstract:*** *In a two-phase flow, the phases can be arranged in different flow patterns depending on pipeline geometry and each phase's superficial velocities ($J_G$ and $J_L$). The slug flow occurs in many industrial situations, such as nuclear reactors, oil extraction from wells, and power plants, among other applications. The upward vertical slug pattern is characterized by concentric elongated bubbles followed by an aerated liquid slug, creating a quasi-periodic flow. The bubble and tube have almost the same diameter. Due to the wide practical use, it is clear the importance of developing studies to better understand the slug flow characteristics along the pipe. Different from horizontal flows, vertical flows need a longer length to reach a fully developed flow. There are few experimental data involving air-water flow in vertical pipes with more than one measurement point along the line in the literature. Even in these studies, the test section is short. This paper aims to study the progression of the slug flow of air-water in a long vertical test section. The experiment was carried out on a line of ID 23.4 mm and a dimensionless length of 1,434D. The experimental setup has three stations equipped with pressure sensors. The pressure sensor measures the pressure gradient, and the void fraction is determined using the quick close valves technique. The experimental results are compared with a semi-analytical model to assess the model's prevision capabilities. The drift relation for the data is analyzed. The numerical model agreed with the experimental data from a long vertical test section, showing less than a 5% deviation for the pressure gradient.*
***Keywords:*** *slug flow, air-water flow, pressure gradient, void fraction.*

## 1. INTRODUCTION

When two fluids flow in a pipe, the phases can arrange in different flow patterns depending on the pipe configuration and each fluids' superficial velocities. Many authors described the flow patterns for vertical two-phase in literature. Four of them are consensual for all authors: bubble, slug, churn, and annular (Hewitt & Hall-Taylor, 1970; Taitel et al., 1980). Among all, the slug flow has great importance because it occurs in many industrial situations, such as nuclear reactors, oil extraction from wells, chemical and space industry, and power plants (Fernandes et al., 1983; Rodrigues et al., 2007; Saidj et al., 2018; Shoham, 2006). Due to the wide practical use, it is clear the importance of developing studies to better understand the flow characteristics of the slug pattern.

The slug flow consists of an elongated bullet-shaped bubble followed by an aerated liquid slug. The elongated bubble is concentric in vertical flow, and its diameter is almost equal to the pipe. If the gas expansion effect is neglected, the flow is periodically formed by a sequence of unit cells. The concept of a unit cell was first introduced by (Wallis, 1969) and employed by many authors to develop their slug flow models (Andreussi et al., 1993; Cook & Behnia, 1997; Dukler & Hubbard, 1975; Fernandes et al., 1983; Nicholson et al., 1978; Sylvester, 1987; Taitel & Barnea, 1990). While the other models were proposed for horizontal and inclined flows, (Fernandes et al., 1983; Sylvester, 1987) proposed the model for vertical flows, but without the gas expansion effect. Therefore, all cells have the same characteristics throughout the line. This is reasonable for horizontal and slightly inclined flows; however, the gas expansion can be significant for vertical flows.

(Fernandes et al., 1983) was the first to propose a specific model for vertical flow. The authors validated the model with data from air-water slug flow in a vertical pipe of 50.74 mm ID and 11.1 m (219D). The authors showed the pressure drop in the slug calculating procedure. However, the authors did not compare the pressure drop prediction with experimental data. The model had good prediction capabilities with a 2.5% mean deviation for the void fraction. Although this model presented good results, the authors only validated the results for short dimensionless length pipes. (Brito et al., 2018) reported that the gas expansion effect is small for their experiment's 246D vertical test section. Nonetheless, the gas expansion effect can be significant for long pipes.

(Sylvester, 1987) developed a model based on Fernandes' model and studied the predictions capabilities for pressure drop in oil-gas and water-gas flows. The author presented water-gas and oil-gas flow data. The pipe geometry for water-gas was ID spanning from 26.670 to 40.894 mm and pipe length spanning from 279.806 to 435.254 m, while for oil-gas flow was ID spanning from 35.052 to 75.997 mm and pipe length spanning from 279.806 to 3,793.540 m. The mean

pressure drop deviation of both cases is 4.83%. Although the author compared his model with data of long pipes, it is complex to assure slug flow throughout the entire line. Also, the author did not present an uncertainty analysis of the field data used to validate his model.

(Mi et al., 2001) studied the air-water slug flow characteristics in a vertical section of 59D using an impedance void meter and signal processing. The authors mention that this pipe configuration is insufficient to reach a fully developed flow. Unlike horizontal flows, vertical flows need a longer development length. According to (Morgado et al., 2016), a developed flow has no interaction between the elongated bubbles or coalescence. (Liu, 1993) reported entrance length spanning from 60D to 100D for vertical. (Saidj et al., 2018) confirmed Liu's statement carrying out experiments in a vertical test section of 176D, with the flow being developed after 95D.

Most of the data available in the literature are for short vertical lines with a length spanning from 35D to 246D, and, therefore, it is not sure that the developed flow is obtained (Brito et al., 2018; Fernandes et al., 1983; Jaeger et al., 2018; Lu et al., 2018; Mao & Dukler, 1989; Mi et al., 2001; Saidj et al., 2018; Santos, 2007; Wang et al., 2021; Zhang et al., 2018). And only a few of the experimental studies were done with more than one measurement station along the line.

This paper aims to study the pressure gradient of air-water slug flow in a vertical pipe of 23.4 mm ID and 1,434D dimensionless long. This study is motivated by the lack of experimental data on long vertical lines and models that consider gas expansion. The experimental results are compared with a semi-analytical model. The empirical drift relation for the data is also analyzed.

This paper is organized as follows: Section 2 describes the experimental apparatus; Section 3 presents the semi-analytical model, the pressure drop of a unit cell, and the equations needed; Section 4 presents the results and discussion of the study; The conclusion is shown in section 5.

## 2. EXPERIMENTAL SETUP

An experimental apparatus was assembled for vertical multiphase studies at Flow&Rs Lab, a facility specially designed for vertical flow experimental studies. The Flow&Rs Lab is a 40 m tall building distributed with ten floors and easy access to the lines. Therefore, it's easy to assemble any instrumentation. The communication infrastructure allows instruments to integrate with a computer-based control system with a low effort. The experimental apparatus consists of water and air loops, three instrumentation stations along the line, a water pump and compressed air stations, and a flow measurement station, as shown in Fig. 1. The line is fully instrumented, and Tab. 1 shows the range and accuracy of all instruments. The apparatus is controlled using a SCADA (Supervisory Control and Data Acquisition) system specially developed using LabVIEW.

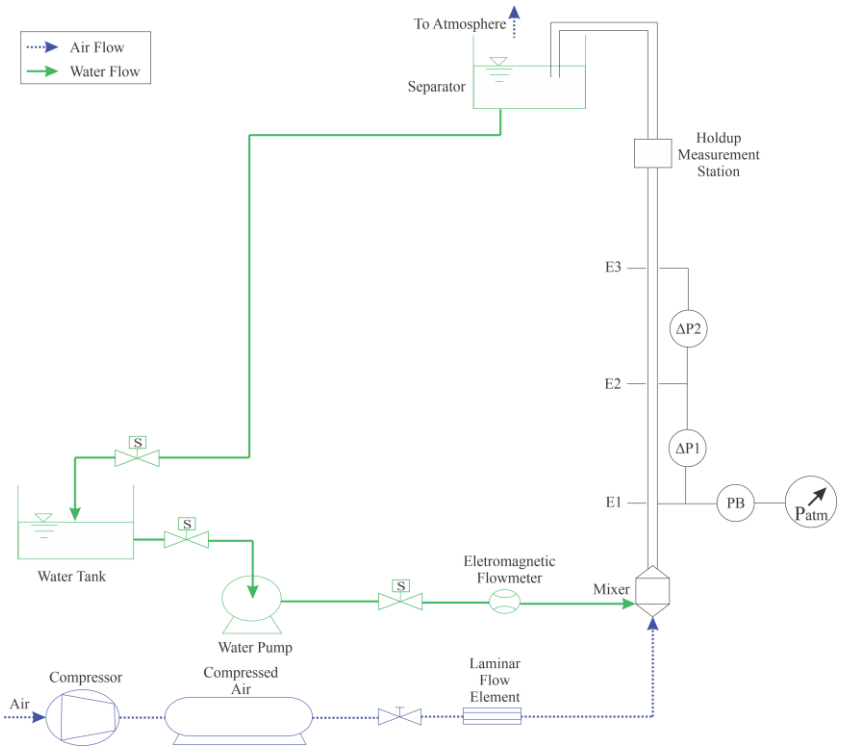


Figure 1. **Experimental facility; hydraulic circuit (→), and pneumatic circuit (⇢).**

The experimental apparatus extends from the ground to the 8th floor at Flow&Rs Lab. A centrifugal pump and a screw compressor are located on the ground floor and supply the water and air. A Rosemount 8750W magnetic flowmeter measures the water flow rate. The flow rate is controlled using the pump's frequency inverter (WEG CFW-50) and a pneumatic controlled globe valve (Fisher Baumann 24000CVF). The mass airflow rate is measured by a laminar flow

element (LFE) plus pressure and temperature transducers at LFE's entrance. The LFE is Merian model 50MJ10, and it's used a Rosemount 2051 pressure sensor to measure the pressure drop at LFE. The pressure and temperature at LFE's entrance are measured by a Rosemount 2051 and SMAR TT301 transducer. The air mass flow rate is manually controlled using a mechanical air pressure regulator (JELPC model BRF 4000) and a Swagelok needle valve. The pressure transducers are differential, and the local atmospheric pressure is measured by a ZÜRICH Z.10.BAROMETRO.420.

Table 1. **Equipment's range and accuracy.**

| Equipment | Localization | Range | Accuracy |
|---|---|---|---|
| Rosemount 8750W | Waterline | $3x10^{-4}$ to $3.1x10^{-3}$ [$m^3/s$] | 0.25% of the rate |
| Merian 50MJ10 | Airline | $2.25x10^{-4}$ to $1.59x10^{-3}$ [$m^3/s$] | ±0.8% |
| SMAR LD301 | Test section | -50 to 50 [kPa] | 0.1% of the span |
| Rosemount 2051 | Test section | -50 to 50 [kPa] | 0.065% of the span |
| | Airline: LFE entrance | 0 to 1,200 [kPa] | |
| | Holdup Station | 0 to 19.21 [kPa] | |
| SMAR TT301 | Airline: LFE entrance | 0 to 60 [ºC] | ±0.2 [ºC] |
| ZÜRICH Z.10 | | 0 to 101.3 [kPa] | 0.1% of the span |

The test section is 33.55 m (1,434D) long and was made of stainless steel OD tube with 23.4 mm ID. Three measuring stations are positioned along the test sections at 3.02 m (129D), 11.42 m (488D), and 19.30 m (825D) from the injector. Each station is equipped with pressure transducers. The first station has two pressure transducers; one measures the total pressure at the line bottom (PB) and the other the pressure drop between the first and second stations (ΔP1). The two other stations measure only the pressure drop. The absolute pressure at each measuring station is calculated using the measured bottom and differential pressure. The specific mass is calculated using the absolute pressure, the inlet temperature, and the air's thermodynamic state equation. The pressure transducer in stations 1 and 3 is SMAR LD301, and in station 2 is 2051 Rosemount. The pressure is sampled at 3 kHz using a National DAQ system model NI CDAQ-9185.

The volumetric average void fraction is measured 8.10 m after the third measuring station using the quick closing ball valves technique. The valves are 2.05 m apart, and the void fraction is calculated using a 2051 Rosemount pressure transducer. The pressure tap is 1.951 m apart; therefore, the void fraction spans from 0.02 and 0.98, and the uncertainty is 1.71%. Only one electrical switch operates the two quick valves to avoid human error. The test section has a bypass to minimize the disturbance during the measurement procedures. The bypass is isolated by two normally closed quick closing valves from the test section. All the valves are operated in a prefixed sequence and synchronized to minimize the flow disturbance and avoid water hammers.

The flow is confined when the main quick balls valves close, and then the separation process starts. The separation process is almost instantly because of the high water and air density difference. A few seconds later, a pneumatic quick ball valve opens to assure that the air portion is at atmospheric pressure. Figure 2 shows a schematic before (a) and after (b) the valves are closed.

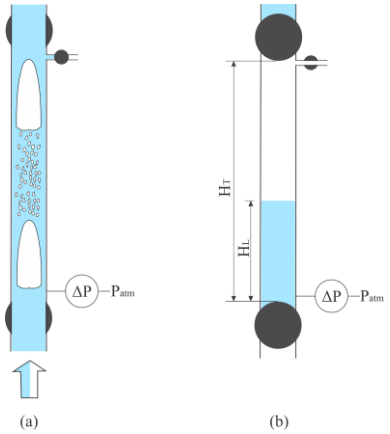


Figure 2. **Schematic of void fraction meter; open valves (a) and closed valves (b).**

The pipe diameter is constant throughout the line, and the volumetric void fraction is:

$$\alpha = \frac{H_T - H_L}{H_T}, \tag{1}$$

where $H_T$ is the distance between the two valves, and $H_L$ is the distance of the liquid-air interface measured from the bottom valve. The liquid-air interface is easily calculated by differential pressure as:

$$H_L = \frac{\Delta P}{g\left(\rho_L - \rho_G\right)} + \frac{\rho_L}{\left(\rho_L - \rho_G\right)} h - \frac{\rho_G}{\left(\rho_L - \rho_G\right)} H_T \,, \tag{2}$$

where $\Delta P$ is the measure differential pressure at the sensor, $g$ is the acceleration due to gravity, $\rho_L$ and $\rho_G$ are the liquid and gas densities, and $h$ is the distance between the valve and the pressure tap. Finally, the volumetric void fraction is:

$$\alpha = 1 - \frac{\Delta P}{g\left(\rho_L - \rho_G\right) H_T} - \frac{\rho_L}{\left(\rho_L - \rho_G\right)} \frac{h}{H_T} + \frac{\rho_G}{\left(\rho_L - \rho_G\right)} \,. \tag{3}$$

## 3. SEMI-ANALYTICAL MODEL

A unit cell consists of an elongated bubble followed by an aerated liquid slug (Wallis, 1969). Figure 3 shows a single cell of slug flow in a vertically oriented pipe. The dotted line represents a control volume moving with the bubble translational velocity; thus, it is possible to consider a steady-state problem.

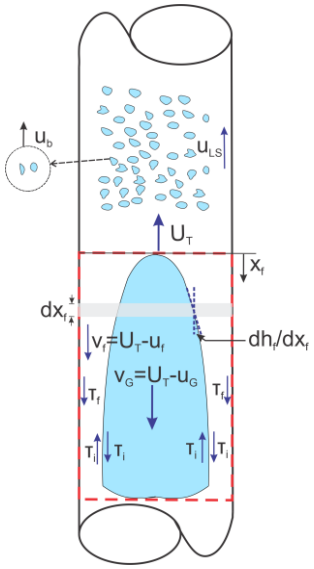


Figure 3.**The unit cell of a slug flow in a vertical pipe.**

The variables in Fig. 3 follow a nomenclature: $U$ is the absolute velocity; $v$ is the relative velocity measured using a reference moving with the bubble nose velocity $\left(U_T\right)$; $\tau$ is the shear stress tensor. The subscript $b$, $LS$, $G$, $f$, and $i$ refer to the dispersed bubble, liquid slug, gas, liquid film, and gas-liquid interface.

The following equations give the mass balances applied to the liquid film and gas phase.

$$\left(U_T - u_{LS}\right) R_S = \left(U_T - u_f\right) R_f \,, \tag{4}$$

$$\left(U_T - u_b\right) \alpha_S = \left(U_T - u_G\right) \alpha_G \,, \tag{5}$$

where: $R_S$ and $R_f$ are the liquid slug, and liquid film holdup; $\alpha_G = 1 - R_f$ and $\alpha_S = 1 - R_S$ are the void fraction in the Taylor bubble and liquid slug.

From the mass balances and momentum equations for each phase, (Taitel & Barnea, 1990) presented the liquid film model differential equation. Equation (6) show this equation for the vertical case.

$$\frac{d}{dx_f} h_f\left(x_f\right) = - \frac{\dfrac{S_f}{A_f}\dfrac{\tau_f}{\rho_f} - \left(\dfrac{1}{A_G} + \dfrac{1}{A_f}\right) S_i \dfrac{\tau_i}{\rho_f} + \left(\dfrac{\rho_f - \rho_G}{\rho_f}\right) g}{\left(\dfrac{v_f^2}{R_f} + \dfrac{\rho_G}{\rho_f}\dfrac{v_G^2}{\alpha_G}\right) \dfrac{d}{dh_f} R_f\left(x_f\right)} \,, \tag{6}$$

where: $h_f$ and $x_f$ are the liquid film thickness and distance from the bubble nose; $S_f$ and $S_i$ are the film and interfacial perimeter; $A_f$ and $A_G$ are the liquid film and gas cross-section area. Due to the symmetry of the Taylor bubble in vertical flows, the geometrical relationship is straightforward with the film thickness. Equations (7) to (10) can be used both for the average and local values.

$$R_f = \frac{4h_f(D-h_f)}{D^2}, \tag{7}$$

$$A_G = \frac{\pi(D-2h_f)^2}{4}, \tag{8}$$

$$S_f = \pi D, \tag{9}$$

$$S_i = \pi\left(D-2h_f\right). \tag{10}$$

The equation (6) is evaluated using geometrical and constitutive closure relationships. Table 2 shows the constitutive relationships used on the liquid film model.

Table 2. **Summary of closure relations.**

| Relation | Equation | Equation |
|---|---|---|
| Liquid film shear stress | $\tau_f = 0.5Cf\,\rho_L u_f\left\|u_f\right\|$ | (11) |
| Interfacial shear stress | $\tau_i = 0.5Cf_i\,\rho_L\left(u_G-u_f\right)\left\|u_G-u_f\right\|$ | (12) |
| Fanning friction factor | $\frac{1}{\sqrt{Cf}} = -4\log_{10}\left(\frac{\in/D}{3.7}+\frac{1.256}{\mathrm{Re}\sqrt{Cf}}\right)$ | (13) |
| Friction factor at the gas-liquid interface | $Cf_i = 0.005\left(1+300\frac{h_f}{D}\right)$ | (14) |
| Liquid slug void fraction | $\alpha_S = \frac{J_G}{C_2+C_3J}$<br>$C_2 = 0.425$<br>$C_3 = 2.65$ | (15) |
| Drift | $V_{drift} = 1.53\left(\frac{\sigma g\Delta\rho}{\rho_L^2}\right)^{0.25}\left(1-\alpha_S\right)^{1.75}$ | (16) |
| Translational bubble velocity | $U_T = 1.2J+0.35\sqrt{gD}$ | (17) |
| Liquid slug dispersed bubble velocity | $u_b = C.J+V_{drift}$<br>$C=1$ | (18) |

Note: Equation (13) is from (Colebrook, 1939), Eq. (14) is from (Wallis, 1969), Eq. (15) is the correlation proposed by (Sylvester, 1987) and the constants are from the fit with the Fernandes' experimental data, Eq. (16) is from (Harmathy, 1960), Eq. (17) is from (Bendiksen, 1984), and Eq. (18) is the drift relation proposed by (Zuber & Findlay, 1965).

Equation (6) is integrated along the liquid film length until the liquid film length is reached. A straightforward way to establish the liquid film length is using slug a frequency correlation. There are many frequency correlations for horizontal flows, but none can be applied to vertical flows. An alternative to determine the liquid film length is:

$$\frac{L_F}{D} = \frac{\beta}{\left(1-\beta\right)}\frac{L_S}{D}, \tag{19}$$

where $L_S$ is the liquid slug length and $\beta$ is the intermittency factor. (Sylvester, 1987) suggested the value of 40D to the liquid slug, while (Taitel et al., 1980) reported a stable slug length of 16D for air-water flows. The intermittency factor is determined using a gas and liquid mass balance over the cell as:

$$J_G = \beta\alpha_G u_G + \left(1-\beta\right)\alpha_S u_b, \tag{20}$$

$$J_L = (1-\beta) R_S u_{LS} + \beta R_f u_f , \tag{21}$$

where $J_L$ and $J_G$ are the liquid and gas superficial velocities.

The unit cell model has limitations because it assumes that the flow is periodic, with no cell interactions, and that the cells are equal throughout the pipe. However, the gas expands along the line as the pressure drops and the unit cell length increases.

The total pressure drops between two points on upward vertical slug flow consist mainly of gravitational and frictional components. The frictional pressure drop along a single cell is divided into three parts, as shown in Fig. 4: liquid slug $(\Delta P_S)$, back of the bubble $(\Delta P_{Mix})$, and liquid film (Wallis, 1969). The frictional pressure drop on the film region balances with the frictional pressure at the gas-liquid interface. Therefore, the pressure in the liquid film or inside the Taylor bubble is constant (Morgado et al., 2016). The $\Delta P_{Mix}$ is due to the turbulence at the back of the bubble. The unit cell model does not consider the interaction between cells and, therefore, neglects that pressure drop. Consequently, the frictional pressure drop is located only at the liquid slug. The frictional liquid slug pressure drop is:

$$\Delta P_S = 4\tau \frac{L_S}{D} , \tag{22}$$

where de shear stress is:

$$\tau = C f_M \frac{\rho_M J |J|}{2} . \tag{23}$$

and $J = J_G + J_L$ is the superficial mixture velocity, and the subscript *M* refers to the mixture. In the liquid slug, the gas distribution is homogeneous along with the liquid slug. Therefore the mixture fluid properties use the homogenous model. The friction factor is calculated using the Colebrook friction factor correlation using the mixture's Reynolds number.

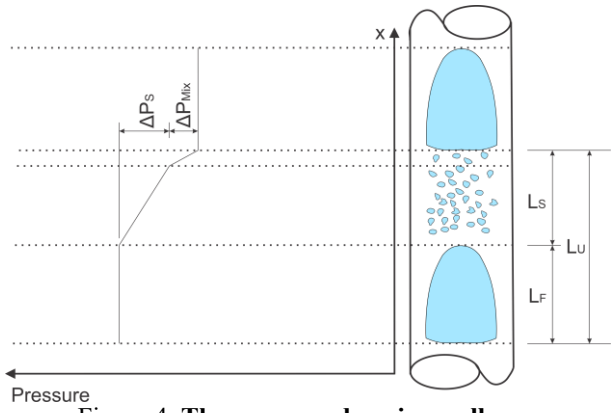


Figure 4. **The pressure drop in a cell.**

The gravitational pressure component is the hydrostatic pressure acting throughout the cell and is determined by:

$$\Delta P_{hydrostatic} = \rho_U g \left( \frac{L_U}{D} \right) D , \tag{24}$$

where $\rho_U$ is the unit cell's density determined as:

$$\rho_U = \alpha_U \rho_G + (1-\alpha_U) \rho_L , \tag{25}$$

with:

$$\alpha_U = \beta \alpha_G + (1-\beta) \alpha_S . \tag{26}$$

The gas density is assumed to be constant along with the cell.

Equations (4) to (26) constitute the model, and all the equations are solved simultaneity to obtain all the cell's parameters in a march process from the beginning until the line's end. The pressure and superficial velocities at the first

measuring station are used as the initial boundary condition. From the pressure and the measured mass gas flow rate, the gas's superficial velocity at station 1 is:

$$J_G^{E1} = \frac{Q_G^{lam}}{A}\frac{P_{lam}}{P_B}, \tag{27}$$

where $Q_G^{lam}$ is the measured flow rate using the LFE, $P_{lam}$ and $P_B$ is the absolute pressure measured at the LFE entrance and the first measuring station. It's assumed to be an isothermal flow and that the air behaves like a perfect gas. The liquid is incompressible, and therefore the liquid superficial velocity is obtained using the measured liquid flow rate and pipe diameter.

## 4. RESULTS AND DISCUSSION

Choosing a grid test for vertical slug flow isn't an easy task because it is desirable slug flow throughout the entire line. Furthermore, the experimental points are limited by the experimental facility measuring and pumping capacities. The flow map proposed by (Taitel et al., 1980) was used to help with this task. Table 3 shows the superficial velocities for all tested points, and Fig. 5 shows them on Taitel's flow map. The Froude and Reynolds numbers are defined using the mixture properties, and the superficial gas velocity is calculated at local atmospheric pressure. The experimental grid has all points upper the critical Froud value of 3.5, but #1. Thus, the test grid selected covers the two Froude ranges reported in the literature: $Fr > 3.5$ and $Fr < 3.5$. The Reynolds spans from $3.3\text{x}10^4$ to $6.4\text{x}10^4$, featuring a turbulent regime that is the industry's primarily flow regime. It's was used the homogeneous model with atmospheric gas velocity to calculate the mixture properties.

Table 3. **Experimental test grid.**

| Test # | $J_L$ [m/s] | $J_G$ [m/s] | J [m/s] | $Fr = \frac{J}{\sqrt{gD}}$ | $Re = \frac{\rho_M J D}{\mu_M}$ |
|---|---|---|---|---|---|
| 1 | 0.3 | 1.2 | 1.5 | 3.1 | $3.30\text{x}10^4$ |
| 2 | 0.3 | 2.3 | 2.6 | 5.4 | $5.41\text{x}10^4$ |
| 3 | 0.6 | 1.5 | 1.8 | 4.4 | $4.72\text{x}10^4$ |
| 4 | 0.6 | 2.3 | 2.9 | 6.1 | $6.39\text{x}10^4$ |

All the experimental points were in the slug region according to Taitel's flow map if the dimensionless entrance length for churn flow is 250. The entrance length is the liquid slug stable length and the intermittence factor function. (Taitel et al., 1980) suggested that the entrance length can span from 50 to 500.

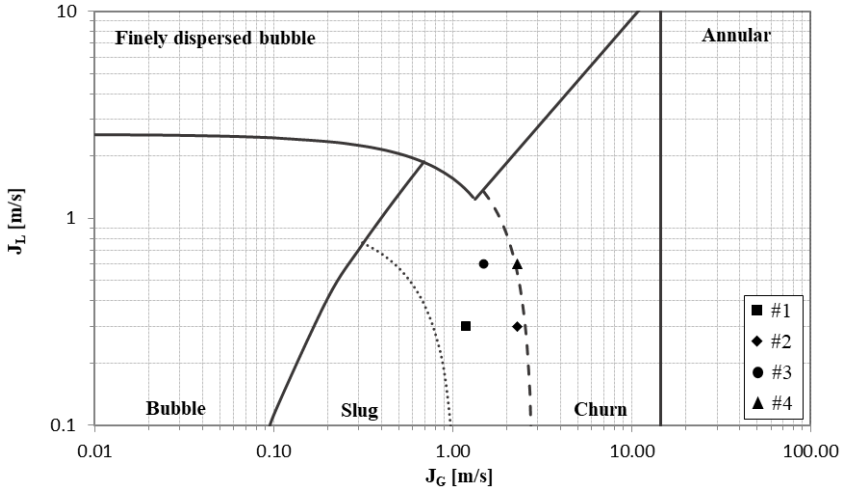


Figure 5. **Experimental test grid; pattern transition (——), $L_E/D = 100$ (·····), and $L_E/D = 250$ (----).**

The averaged void fraction measured using the quick close valves technique for all tested points is shown in Tab. 4. The uncertainty analysis of the experimental data shows a maximum measurement relative error of 1.71% for the void fraction. The void fractions span from 0.54 to 0.75, while the injection fraction $\left(J_G/J\right)$ is higher and spans from 0.71 to 0.88. This is typical for slug flow behavior and indicates a slippage between the gas and liquid phases. The table also shows the standard deviation, the coefficient of variation, and the number of repetitions. The number of repetitions was determined to ensure a 95% confidence interval and 5% margin of error. As the sample size is small, it was considered

that the sample follows the Student's t-distribution. Even having more repeats, runs #2 and #4 have the highest CV values. These runs have the highest gas flow rates causing large bubbles and more aerated liquid slugs. The probability of catching only one large and no representative bubble when the quick valve close increases and requires more repetitions.

Table 4. **Experimental average void fraction.**

| Test # | $J_G/J$ | Void Fraction | s | CV [%] | Repetitions |
|---|---|---|---|---|---|
| 1 | 0.80 | 0.66 | 0.063 | 9.52 | 19 |
| 2 | 0.88 | 0.75 | 0.084 | 11.25 | 24 |
| 3 | 0.71 | 0.54 | 0.049 | 9.00 | 15 |
| 4 | 0.79 | 0.62 | 0.070 | 11.34 | 26 |

One of the most well-known slug flow characteristics is the drift relationship representing the slug flow signature. This relationship was first proposed by (Zuber & Findlay, 1965) and can be expressed in a dimensionless form as:

$$\frac{J_G}{\alpha\sqrt{gD}} = C_0 Fr + C_\infty , \tag{28}$$

where $C_0$ is the distribution parameter and $C_\infty$ is the drift coefficient. The distribution parameter represents the mixture's relationship to the liquid's maximum velocity on the liquid slug ahead of the bubble. The drift velocity means the slippage between the gas and liquid phases, representing the bubble velocity over a stagnated liquid. According to several authors (Bendiksen, 1984; Choi et al., 2012; Taitel & Barnea, 1990; Zuber & Findlay, 1965; Alves et al., 1993), the distribution is 2.0 when the flow is laminar and spans from 1 to 1.2 for turbulent flows. The drift parameter is 0.35. Figure 6 shows the drift relationship measured in the void fraction meter. The distribution parameter was determined by a linear regression using the measured void fraction and superficial gas velocity, with the drift parameter fixed to 0.35. The superficial gas velocity at the void fraction meter was estimated as:

$$J_G = \frac{Q_G^{lam}}{A}\frac{P_{lam}}{P_{E3} - (dP/dL)\Delta L} , \tag{29}$$

where $P_{E3}$ is the measured pressure at the third measuring station, $(dP/dL)$ is the measured pressure gradient, and $\Delta L$ is the distance from the third station to the center of the void fraction meter. The drift parameter was fixed because it's challenging to measure it accurately. The drift parameter is calculated by measuring the velocity of released bubbles with different volumes in a stagnated liquid or in a low range flow rate liquid single-phase. It's an arduous task to do it in a complex line, as this study used. Furthermore, this drift parameter value has been reported in numerous studies. And this is the methodology used by several authors to obtain the drift relationship. The result of the linear fit using the experimental data shows a value of $C_0 = 1.114$, which agrees with the distributions parameter range reported. Therefore, it`s reasonable to assume that the flow pattern refers to a slug flow.

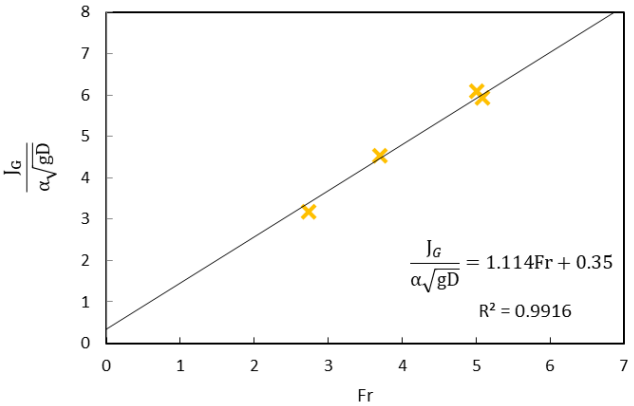


Figure 6. **Empirical drift relation for experimental data.**

Figure 7 shows the numerical void fraction against experimental comparison. The numeric void fraction is determined by integrating Eq. (6), plus Eq. (26). The liquid slug void fraction uses (Sylvester, 1987), and the model calculates the intermittency factor. It's used a cell calculated near the hold up measuring for the comparison. The measured and numerical void fraction has less than 10% deviation. Even though the deviation is higher than the measured error, the numerical results are close to the experimental data and show an excellent prevision capability for a simple model.

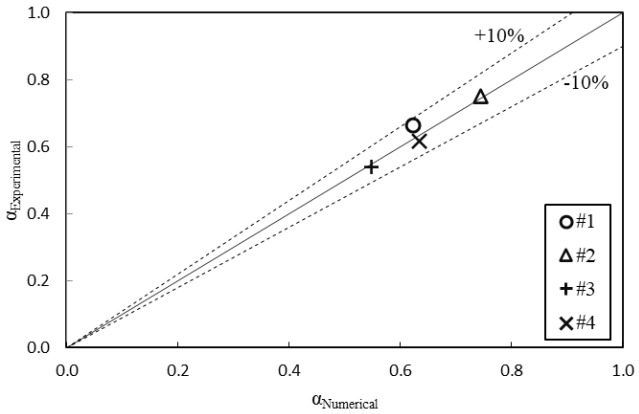


Figure 7. **Comparison of numerical and experimental void fractions.**

The friction pressure gradient determination needs to measure the gravitational component of the pressure accurately. This task requires measuring the void fraction between the pressure taps and two pressure sensors with high accuracy at the low range. For this reason, only the total pressure is presented. Figure 8 compares the measured and numerical total pressure gradient. The deviation is less than 5%, and the uncertainty analysis of pressure shows a maximum relative error of 2.11%. The numerical model obtains good results, even being such a simple model. And the differences can be caused by some considerations and approximations in the numerical model. The model neglected the pressure drop due to the turbulence at the bubble rear $\left(\Delta P_{Mix}\right)$, and the stable piston length of 16D for all runs can also be an error source.

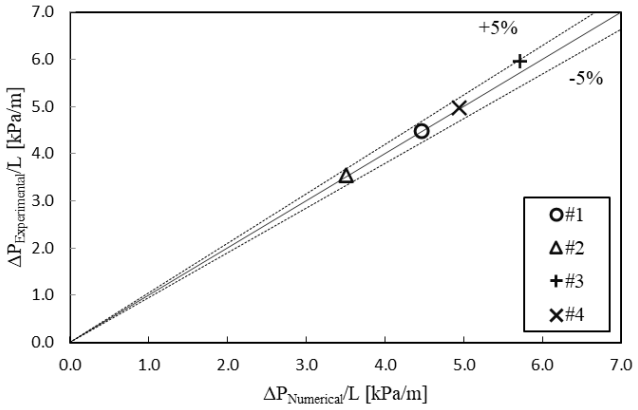


Figure 8. **Numerical versus experimental pressure gradient.**

## 5. CONCLUSIONS

A semi-analytical model based on the unit cell model is presented. The numerical results for pressure gradient and average void fraction were compared with experimental data of a long vertical pipe. The drift relation using the experimental data shows a distribution parameter $C_0 = 1.114$, which agrees with the values described in the literature. The model's prediction for the void fraction is close to experimental measured by the quick close valves technique. The deviation is less than 10% error. The pressure gradient agreed with the experimental data with less than 5% deviation. Given the simplicity of the semi-analytical model, its presented promising results in predicting the pressure gradient and average void fraction for the long vertical test section.

## 6. ACKNOWLEDGEMENTS

The authors acknowledge the financial support from PETROBRAS/FUNCAMP, under contracts 5302 and 5303. This study was financed in part by the Coordenação de Aperfeiçoamento de Pessoal de Nível Superior - Brasil (CAPES) - Finance Code 001.

## 7. REFERENCES

Andreussi, P., Bendiksen, K. H., & Nydal, O. J. (1993). Void distribution in slug flow. *Int. J. Multiphase Flow*, *19*(5), 817–828.

Bendiksen, K. H. (1984). An experimental investigation of the motion of long bubbles in incline tubes. *Int. J. Multiphase*

*Flow*, *10*(4), 467–483.
Brito, R., Pereyra, E., & Sarica, C. (2018). Well trajectory effect on slug flow development. *Journal of Petroleum Science and Engineering*, *167*, 366–374. https://doi.org/10.1016/j.petrol.2017.07.050
Choi, J., Pereyra, E., Sarica, C., Park, C., & Kang, J. M. (2012). An efficient drift-flux closure relationship to estimate liquid holdups of gas-liquid two-phase flow in pipes. *Energies*, *5*(12), 5284–5306. https://doi.org/10.3390/en5125294
Colebrook, C. F. (1939). Turbulent flow in pipes, with particular reference to the transition region between the smooth and rough pipe laws. *Journal of the Institution of Civil Engineers*, *11*(4), 133–156.
Cook, M., & Behnia, M. (1997). Film profiles behind liquid slugs in gas-liquid pipe flow. *AIChE Journal*, *43*(9), 2180–2186.
Dukler, A. E., & Hubbard, M. G. (1975). A model for gas-liquid slug flow in horizontal and near horizontal tubes. *Ind. Eng. Chem.*, *14*(4), 337–347.
Fernandes, R. C., Semiat, R., & Dukler, A. E. (1983). Hydrodynamic model for gas-liquid slug flow in vertical tubes. *AIChE Journal*, *29*(6), 981–989. https://doi.org/10.1002/aic.690290617
Harmathy, T. Z. (1960). Velocity of large drops and bubbles in media of infinite or restricted extent. *AIChE Journal*, *6*(2), 281–288.
Hewitt, G. F., & Hall-Taylor, N. S. (1970). *Annular two-phase flow*. Pergamon Press. https://doi.org/10.1016/0017-9310(72)90222-0
Jaeger, J., Santos, C. M., Rosa, L. M., Meier, H. F., & Noriler, D. (2018). Experimental and numerical evaluation of slugs in a vertical air–water flow. *International Journal of Multiphase Flow*, *101*, 152–166. https://doi.org/10.1016/j.ijmultiphaseflow.2018.01.009
Liu, T. J. (1993). Bubble size and entrance effects on void development in a vertical channel. *Int. J. Multiphase Flow*, *19*(1), 99–113.
Lu, C., Kong, R., Qiao, S., Larimer, J., Kim, S., Bajorek, S., Tien, K., & Hoxie, C. (2018). Frictional pressure drop analysis for horizontal and vertical air-water two-phase flows in different pipe sizes. *Nuclear Engineering and Design*, *332*, 147–161. https://doi.org/10.1016/j.nucengdes.2018.03.036
Mao, Z. S., & Dukler, A. E. (1989). An experimental study of gas-liquid slug flow. *Experiments in Fluids*, *8*(3–4), 169–182. https://doi.org/10.1007/BF00195792
Mi, Y., Ishii, M., & Tsoukalas, L. H. (2001). Investigation of vertical slug flow with advanced two-phase flow instrumentation. *Nuclear Engineering and Design*, *204*, 69–85. https://doi.org/10.1016/S0029-5493(00)00326-5
Morgado, A. O., Miranda, J. M., Araújo, J. D. P., & Campos, J. B. L. M. (2016). Review on vertical gas–liquid slug flow. *International Journal of Multiphase Flow*, *85*, 348–368. https://doi.org/10.1016/j.ijmultiphaseflow.2016.07.002
Nicholson, M. K., Aziz, K., & Gregory, G. A. (1978). Intermittent two phase flow in horizontal pipes predictive models. *The Canadian Journal of Chemical Engineering*, *56*, 653–663.
Rodrigues, H. T., Morales, R. E., Mazza, R. A., & Rosa, E. S. (2007). A comparitive study of closure equations for gas-liquid slug flow. *19th International Congress of Mechanical Engineering*, 9.
Saidj, F., Hasan, A., Bouyahiaoui, H., Zeghloul, A., & Azzi, A. (2018). Experimental study of the characteristics of an upward two-phase slug flow in a vertical pipe. *Progress in Nuclear Energy*, *108*, 428–437. https://doi.org/10.1016/j.pnucene.2018.07.001
Santos, T. S. M. M. (2007). *Hydrodynamics of gas liquid flows in slug flow regime* [Universidade do Porto]. http://hdl.handle.net/10216/11060
Shoham, O. (2006). *Mechanistic modeling of gas-liquid two-phase flow in pipes*. Society of Petroleum Engineers.
Sylvester, N. D. (1987). A mechanistic model for two-phase vertical slug flow in pipes. *Journal of Energy Resources Technology*, *109*, 206–213. https://doi.org/doi.org/10.1115/1.3231348
Taitel, Y., & Barnea, D. (1990). Two-phase slug flow. *Advances in Heat Transfer*, *20*, 83–132.
Taitel, Y., Barnea, D., & Dukler, A. E. (1980). Modelling flow pattern transitions for steady upward gas-liquid flow in vertical tubes. *AIChE Journal*, *26*(3), 345–354.
Wallis, G. B. (1969). *One-dimensional two-phase flow*. McGraw-Hill, Inc.
Wang, T., Gui, M., Zhang, T., Bi, Q., Zhao, J., & Liu, Z. (2021). Experimental investigation on characteristic parameters of air–water slug flow in a vertical tube. *Chemical Engineering Science*, *246*, 1–16. https://doi.org/10.1016/j.ces.2021.116895
Zhang, M., Pan, L. ming, He, H., Yang, X., & Ishii, M. (2018). Experimental study of vertical co-current slug flow in terms of flow regime transition in relatively small diameter tubes. *International Journal of Multiphase Flow*, *108*, 140–155. https://doi.org/10.1016/j.ijmultiphaseflow.2018.07.005
Zuber, N., & Findlay, J. A. (1965). Average volumetric concentration in two-phase flow systems. *Journal of Heat Transfer*, 453–468.

## 8. RESPONSIBILITY NOTICE

The authors are solely responsible for the information included in this paper.